Figure 1. Examples of Live kV images acquired with the XLTS and corresponding CE images obtained for the two projection views of each patient. Tumour contours identified with the XLTS and with the contrast enhancement method are outlined in red and blue, respectively. Lung and mediastinum background regions used to compute the tumour contrast are depicted in green and yellow, respectively.

Table 1. Ratio between the Michelson contrast computed for the CE images and for the corresponding Live projections at different tumour-background interfaces. Results for each patient are expressed as median ± inter-quartile range of the contrast values obtained for all kV images selected in the simulation and treatment fractions.

Patient	$Contrast_{CE} / Contrast_{Live}$			
	VIEW A		VIEW B	
	Tumour-lung	Tumour-mediastinum	Tumour-lung	Tumour-mediastinum
P1	9.0 ± 11.1	7.6 ± 3.8	2.2 ± 0.3	8.6 ± 10.8
P2	2.2 ± 0.1	-	5.3 ± 0.6	-
P3	53.6 ± 262.7	-	2.9 ± 0.8	8.7 ± 4.0
P4	5.9 ± 0.5	-	9.8 ± 14.6	-
P5	6.3 ± 0.7	-	4.7 ± 0.4	-

Conclusions: The potential of the contrast enhancement method in increasing the applicability of markerless lung tumour tracking based on kV imaging was demonstrated on clinical data. A time-resolved (4D) CT scan can be used instead of the breath-hold CT scan available for this study in order to improve the robustness in the background subtraction operation, especially in case of lower lobe tumours for the compensation of diaphragm motion due to breathing.

[1] Yang Y *et al*, IJROBP 2012;82:e749-56.
[2] Spadea MF *et al*, IJROBP 2014;90:628-36.

OC-0550

Feasibility of markerless tumor tracking by sequential dual-energy fluoroscopy on a clinical tumor tracking system

J. Dhont[1], K. Poels[1], D. Verellen[1], K. Tournel[1], M. Boussaer[1], C. Collen[1], B. Engels[1], T. Gevaert[1], F. Steenbeke[1], M. De Ridder[1]

[1]Universitair Ziekenhuis Brussel, Radiotherapy, Brussels, Belgium

Purpose/Objective: The purpose of this study is to evaluate the feasibility of markerless tumor detection using sequential dual-energy fluoroscopy sequences. As fast-switching kilovolt (kV) generators are not readily available, motion artifacts due to a time lapse between high and low energy images are often a cause for concern. For those kV generators without rapid switching, an alternative approach is proposed consisting of using sequential (high and low kV) high frame rate fluoroscopy sequences, already available in the clinical dynamic tracking (DT) workflow of the Vero SBRT system to build the hybrid correlation model.

Materials and Methods: Two sequential 20s (11 Hz) fluoroscopy sequences were acquired at the start of one fraction for 4 patients treated for primary NSCLC with DT on the Vero SBRT system. Two sequences were acquired, using 2 on-board kV imaging systems located at ± 45° from the MV beam axis, at respectively 60 kV (3.2 mAs) and 120 kV (2.0 mAs). Table 1 shows the kV imager positions, which were selected based on marker visibility. Offline, a normalized cross-correlation algorithm was applied to anatomically match the high (HE) and low energy (LE) images. Per breathing phase (inhale, exhale, maximum inhale and maximum exhale), the five best matching HE and LE couples were extracted for dual energy subtraction. A validation on an anthropomorphic phantom with an imposed artificial tumor volume was conducted to validate the dual-energy approach. A contrast analysis according to gross tumor volume (GTV) was conducted between the DE and HE images based on contrast to noise ratio. Improved tumor visibility was quantified in function of 4 breathing phases using an improvement ratio ($IR = CNR_{DE}/CNR_{HE}$).

Results: The additional acquisition of a 60 kV fluoroscopy sequence enabled an unambiguous approach to dual-energy imaging into the clinical workflow. Normalized cross correlation for HE-LE fluoroscopy sequence matching resulted in a mean correlation coefficient of 0.92 ± 0.18 based on the 5 best anatomical HE-LE matches per breathing phase. Contrast to noise ratio's (CNR) per patient can be found in Table 1. Bone suppression by DE subtraction imaging was successful. An example is shown in Figure 1. Based on the CNR, with the exception of one imaging angle the DE images showed no significantly improved tumor visibility compared to the HE images, with an improvement ratio averaged over all patients of 1.00 ± 0.50.
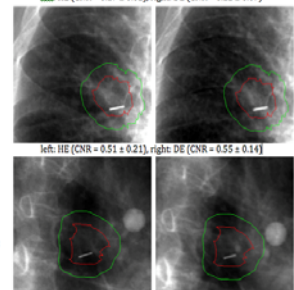
Conclusions: Dual-energy subtraction imaging by sequential orthogonal fluoroscopy was shown feasible by implementing an additional LE fluoroscopy sequence into the DT workflow. However, for most imaging angles, dual-energy images showed no significantly improved tumor visibility over HE imaging.

Table 1 Contrast to noise ratio and improvement ratio according to gross tumor volume (GTV) between the dual and high-energy images per patient.

	CNR SD		Improvement ratio
	HE	DE	
patient 1 Im. 1 - 35°	0.53 ± 0.15	0.21 ± 0.08	0.41 ± 0.10 p = 0.057
patient 1 Im. 2 - 125°	0.23 ± 0.08	0.40 ± 0.11	1.87 ± 0.63 p = 0.323
patient 2 Im. 1 - 225°	0.17 ± 0.02	0.12 ± 0.07	0.68 ± 0.42 p = 0.090
patient 2 Im. 2 - 315°	0.51 ± 0.21	0.55 ± 0.14	1.14 ± 0.28 p = 0.833
patient 3 Im. 1 - 315°	0.49 ± 0.14	0.63 ± 0.11	**1.42 ± 0.56** **p < 0.005**
patient 3 Im. 2 - 45°	1.07 ± 0.28	0.66 ± 0.05	0.65 ± 0.19 p = 0.005
patient 4 Im. 1 - 78°	0.22 ± 0.08	0.11 ± 0.09	0.57 ± 0.64 p = 0.009
patient 4 Im. 2 - 348°	0.85 ± 0.24	0.99 ± 0.11	1.24 ± 0.26 p = 0.021

Abbreviations: CNR = contrast to noise ratio; SD = standard deviation; HE = high energy; DE = dual energy

Figure 1 Dual energy subtraction images from patient 2, imager 1 (above) and imager 2 (below) (GTV = red contour). left: HE (CNR = 0.17 ± 0.02), right: DE (CNR = 0.12 ± 0.07)

left: HE (CNR = 0.51 ± 0.21), right: DE (CNR = 0.55 ± 0.14)

OC-0551

High spatial and timing resolution silicon based dosimeter for quality assurance of real time adaptive radiotherapy

M.K. Newall[1], M. Petasecca[1], M. Duncan[1], A.H. Aldosari[1], K. Al shukaili[1], C.S. Porumb[1], I. Fuduli[1], J.T. Booth[2], E. Colvill[2], P. Keall[3], M.L.F. Lerch[1], V. Perevertaylo[4], A.B. Rosenfeld[1]

[1]University of Wollongong, Centre for Medical Radiation Physics, Wollongong, Australia
[2]Royal North Shore Hospital, Northern Sydney Cancer Centre, St. Leonards, Australia
[3]University of Sydney, Institute of Medical Physics, Sydney, Australia
[4]02232, SPA-BIT, Kiev, Ukraine

Purpose/Objective: Real-time adaptive radiotherapy aims to improve radiation treatment through re-optimisation of treatment delivery based on patient-specific changes in anatomy and biology during treatments. MLC tracking is one real-time adaptive strategy that applies real-time tumour localisation to adapt the MLC shape during treatment. MLC tracking has been shown to be feasible for prostate cancer treatment on a standard linac, leading to improved tumour dose conformity, reduced rectal dose and improved fidelity of the planned treatment compared to standard delivery. Patient specific quality assurance of MLC tracking treatment is complex due to daily variation in tumour motion track creating new adaptations each day. We propose a high temporal and spatial resolution dosimetry system to verify the performance of MLC tracking.

Materials and Methods: A monolithic silicon detector, known as MagicPlate-512 (MP512), has been developed and comprises 512 pixels arranged in a square array with sensitive volume $0.5\times0.5\times0.1mm^3$ and pitch 2mm. The array allows high resolution dose mapping and dose profiling in 2D. The MP512 is read out by a data acquisition system (DAS) synchronised with the electron gun pulses of the linac for pulse by pulse resolution of the dose delivered by the treatment beam. The detector is embedded in a solid water phantom and installed on a movable platform. The platform is supplied with a patient-specific motion pattern to replicate tumour motion. An electromagnetic positioning system provides real time position information to the MLC tracking software. The dose delivered by a static gantry with MLC defined square fields of sizes 1x1, 2x2 and $3x3cm^2$ is measured by MP512 and compared to EBT3 film for cases without motion, with motion and with motion and MLC tracking enabled. The DAS enables verification of dose variation pulse by pulse for each pixel, providing an insight into beam delivery for optimisation or debugging of a plan.

Results: The beam profiles along the y-axis of the detector are compared to the EBT3 film for the three motion cases for the $2x2cm^2$ MLC defined field.
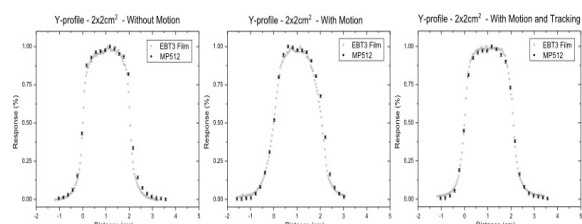
The penumbral width (80-20%) and full-width at half-maximum is measured for each profile for the field sizes and motion cases, the results benchmarked by EBT3 film.

Square Field size (cm^2)	FWHM (cm) +/- 0.01 cm		Penumbral Width (PW) (cm) +/- 0.01	
	MP512	EBT3	MP512	EBT3
without Motion				
1	1.17	1.14	0.25	0.26
2	2.10	2.04	0.30	0.27
3	3.16	3.06	0.29	0.30
with Motion				
1	1.21	1.16	0.51	0.50
2	2.15	2.07	0.56	0.54
3	3.15	3.10	0.57	0.53
with Motion and MLC tracking				
1	1.14	1.10	0.37	0.35
2	2.10	2.10	0.38	0.34
3	3.12	3.10	0.39	0.35

Conclusions: The results measured by the MP512 show excellent agreement with EBT3 film. The motion is observed to smear the profile of the beam. MP512 and EBT3 are able to reconstruct the distortion within 0.2mm; with MLC tracking enabled the smearing is reduced with a good agreement between no-motion and motion-tracking. The MP512 detector has proven to be an effective tool for pre-treatment verification of real-time adaptive deliveries with both high spatial resolution for dose profiling and high temporal resolution for pulse by pulse reconstruction.

Proffered Papers: Physics 10: Dose measurements challenges

OC-0552
First direct comparison of measured kQ values for FFF and FF clinical photon beams

L.A. De Prez[1], B.J. Jansen[1], J.A. De Pooter[1], T.J. Perik[2], F.W. Wittkämper[2]
[1]VSL, Ionizing Radiation Standards, Delft, The Netherlands
[2]Netherlands Cancer Institute, Department of Radiation Oncology, Amsterdam, The Netherlands

Purpose/Objective: The objective of this study was to directly measure and compare k_Q factors [1] of reference type ionization chambers in flattening-filter (FF) and flattening-filter-free (FFF) clinical photon beams with nominal energies of 6 and 10 MV.

Materials and Methods: Eight Baldwin-Farmer type ionization chambers (2×PTW 30013, 3×NE 2571, 3×PTW 30012) were calibrated in terms of absorbed-dose-to-water, D_w, in ^{60}Co at VSL and in four clinical photon beams of 6 and 10 MV, both FF and FFF of an Elekta Versa HD at the Netherlands Cancer Institute. The absorbed-dose-to water was determined with the new VSL water calorimeter, designed for on-site measurements in clinical teletherapy beams (see Figure). Two waterproof ionization chambers (PTW 30013) were directly calibrated inside the water calorimeter thermostat. The other six ionization chambers (not waterproof) were cross-calibrated in a reference phantom against the PTW 30013 chambers. Both the calorimeter and chamber measurements were performed against an external transmission monitor, placed on the accelerator tray. Measurements were corrected for radial non-uniformity due to the lateral beam profile with respect to the measurement point in the water calorimeter and the measurement volume of the ionization chamber.

The FF and FFF beams of the same nominal energy were matched with respect to pdd(10). Based on pdd(10) the measured k_Q factors in the two FFF beams were compared directly with the FF beams of the same nominal energy. Additionally a comparison between k_Q factors in FFF and FF beams based on quality index $TPR_{20,10}$ for both beams was